The Astrophysical Journal Letters, 937:L30 (7pp), 2022 October 1 https://doi.org/10.3847/2041-8213/ac927f

Accelerating Early Massive Galaxy Formation with Primordial Black Holes

Boyuan Liu[1,2] and Volker Bromm[1]
[1] Department of Astronomy, University of Texas at Austin, 2515 Speedway, Stop C1400, Austin, TX 78712, USA; boyuan@utexas.edu
[2] Institute of Astronomy, University of Cambridge, Madingley Road, Cambridge, CB3 0HA, UK
Received 2022 August 28; revised 2022 September 13; accepted 2022 September 16; published 2022 September 27

Abstract

Recent observations with JWST have identified several bright galaxy candidates at $z \gtrsim 10$, some of which appear unusually massive (up to $\sim 10^{11}\,M_{\odot}$). Such early formation of massive galaxies is difficult to reconcile with standard ΛCDM predictions, demanding a very high star formation efficiency (SFE), possibly even in excess of the cosmic baryon mass budget in collapsed structures. With an idealized analysis based on linear perturbation theory and the Press–Schechter formalism, we show that the observed massive galaxy candidates can be explained with lower SFE than required in ΛCDM if structure formation is accelerated/seeded by massive ($\gtrsim 10^{9}\,M_{\odot}$) primordial black holes (PBHs) that make a up a small fraction ($\sim 10^{-6}$–10^{-3}) of dark matter, considering existing empirical constraints on PBH parameters. We also discuss the potential observational signatures of PBH cosmologies in the JWST era. More work needs to be done to fully evaluate the viability of such PBH models to explain observations of the high-z Universe.

Unified Astronomy Thesaurus concepts: Galaxy abundances (574); Dark matter (353); Primordial black holes (1292)

1. Introduction

Understanding the onset of star and galaxy formation at the end of the cosmic dark ages, a few hundred million years after the Big Bang, is one of the key goals of modern cosmology (e.g., Barkana & Loeb 2001; Bromm & Yoshida 2011). With the successful launch of the James Webb Space Telescope (JWST), this formative period of cosmic history is now becoming accessible to direct observations, thus finally testing the theoretical framework of early structure formation. This framework extends the ΛCDM model, which is highly successful in accounting for galaxy formation and evolution following the epoch of reionization (Springel et al. 2006; Mo et al. 2010) to the first billion years after the Big Bang.

The initial JWST imaging via the Cosmic Evolution Early Release Science (CEERS) survey has revealed a population of surprisingly massive galaxy candidates at $z \gtrsim 10$, with inferred stellar masses of $\gtrsim 10^{9}\,M_{\odot}$ (Atek et al. 2022; Finkelstein et al. 2022; Harikane et al. 2022; Naidu et al. 2022; Yan et al. 2022). The current record among these photometric detections reaches out to $z \simeq 16.7$ (Donnan et al. 2022). Such massive sources so early in cosmic history would be difficult to reconcile with the expectation from standard ΛCDM (Boylan-Kolchin 2022; Inayoshi et al. 2022; Lovell et al. 2022), and this includes similarly overmassive (up to $\sim 10^{11}\,M_{\odot}$) galaxy candidates detected at $z \simeq 10$ (Labbé et al. 2022). An important caveat here is that the early release JWST candidate galaxies are based on photometry only, rendering their redshift and spectral energy distribution (SED) fits uncertain (Steinhardt et al. 2022) until spectroscopic follow-up will become available. Part of the seeming discrepancy may also be alleviated by the absence of dust in sources at the highest redshifts, thus boosting their rest-frame UV luminosities (e.g., Jaacks et al. 2018; Ferrara et al. 2022).

It is a long-standing question in cosmology when the first galaxies emerged and how massive they were, going back to the idea that globular clusters formed at the Jeans scale under the conditions immediately following recombination (Peebles & Dicke 1968). The modern view of early structure formation, based on the dominant role of cold dark matter (CDM), posits initial building blocks for galaxy formation that are low mass, of order $10^{6}\,M_{\odot}$, virializing at $z \simeq 20$–30 (Couchman & Rees 1986; Haiman et al. 1996).

Numerous models have been proposed to suppress small-scale fluctuations, thus delaying the onset of galaxy formation to later times, in response to empirical hints for the lack or absence of low-mass objects that are otherwise predicted by CDM models (Bullock & Boylan-Kolchin 2017). An extreme scenario here is the fuzzy dark matter (FDM) model, which assumes ultralight axion-like dark matter particles with corresponding de Broglie wavelengths of ~ 1 kpc (Hui et al. 2017). Quantum pressure would thus prevent the collapse of structure on the scale of dwarf galaxies (e.g., Sullivan et al. 2018).

The opposite effect, deriving models to *accelerate* early structure formation beyond the ΛCDM baseline prediction, as may be required to explain the massive JWST galaxy candidates, is much more challenging. One recent study invokes the presence of an early dark energy (EDE) component, resulting in such an accelerated formation of high-redshift structures (Klypin et al. 2021). Here, we explore a different possibility of boosting the emergence of massive galaxies in early cosmic history with primordial black holes (PBHs), considering the isocurvature perturbations from PBHs that increase the power of density fluctuations in addition to the standard ΛCDM adiabatic mode (i.e., the "Poisson" effect; Carr & Silk 2018). In addition, we assess the scenario in which the most massive galaxies reported in Labbé et al. (2022) form in halos seeded by massive PBHs that are very rare and evolve in isolation at high z (i.e., the "seed" effect; Carr & Silk 2018).

2. PBH Structure Formation

For simplicity, we adopt a monochromatic[3] mass function for PBHs, such that a PBH model is specified by the black hole mass $m_{\rm PBH}$ and fraction $f_{\rm PBH}$ of dark matter in the form of PBHs. We start with the "Poisson" effect (Carr & Silk 2018) in which PBHs produce isocurvature perturbations in the density field on top of the standard adiabatic mode due to the random distribution of PBHs (at small scales). These isocurvature perturbations only grow in the matter-dominated era. As an extension of the formalism in Afshordi et al. (2003), Kashlinsky (2016), and Cappelluti et al. (2022), where PBHs make up all dark matter ($f_{\rm PBH}\sim 1$), now treating $f_{\rm PBH}$ as a free parameter, the linear power spectrum (extrapolated to $a=1$) of dark matter density fluctuations can be written as (Inman 2019; Liu et al. 2022):

$$P(k) = P_{\rm ad}(k) + P_{\rm iso}(k),$$
$$P_{\rm iso}(k) \simeq [f_{\rm PBH} D_0]^2/\bar{n}_{\rm PBH}, \quad (1)$$

where $P_{\rm ad}(k)$ is the standard adiabatic mode in ΛCDM cosmology,[4] $\bar{n}_{\rm PBH} = f_{\rm PBH}\frac{3H_0^2}{8\pi G}(\Omega_{\rm m}-\Omega_{\rm b})/m_{\rm PBH}$ is the cosmic (comoving) number density of PBHs, and D_0 is the growth factor of isocurvature perturbations evaluated at $a=1$, given by Inman (2019):

$$D(a) \simeq \left(1+\frac{3\gamma}{2a_-}s\right)^{a_-} - 1, \quad s=\frac{a}{a_{\rm eq}},$$
$$\gamma = \frac{\Omega_{\rm m}-\Omega_{\rm b}}{\Omega_{\rm m}}, \quad a_- = \frac{1}{4}(\sqrt{1+24\gamma}-1), \quad (2)$$

where $a_{\rm eq}=1/(1+z_{\rm eq})$ is the scale factor at matter–radiation equality with $z_{\rm eq}\simeq 3400$. So far, we have ignored the higher-order (nonlinear) "seed" effect (Carr & Rees 1984; Carr & Silk 2018), as well as mode mixing,[5] lacking a self-consistent linear perturbation theory that can take them into account. Such effects tend to enhance the perturbations induced by PBHs at large scales but suppress structure formation at small scales with nonlinear dynamics around PBHs (Liu et al. 2022). Particularly, we expect linear perturbation theory to break down at a certain (mass) scale $M_{\rm bk}$, overproducing the abundance of structures below $M_{\rm bk}$. We hypothesize $M_{\rm bk}$ to be between $m_{\rm PBH}$ and the mass $M_{\rm B}(m_{\rm PBH}, z)\sim[(z+1)a_{\rm eq}]^{-1}m_{\rm PBH}$ of overdense ($\delta\gtrsim 1$) regions bound to individual PBHs, when they evolve in isolation (Carr & Silk 2018). In light of this, as a heuristic approach, we further impose a conservative cutoff to the isocurvature term in Equation (1) to suppress the power at scales smaller than $M_{\rm bk}\sim m_{\rm PBH}$:

$$P_{\rm iso}(k) = 0, \quad k > (2\pi^2\bar{n}_{\rm PBH}/f_{\rm PBH})^{-1/3}. \quad (3)$$

As examples, Figure 1 shows the power spectra for three models that turn out to be representative in our analysis below (see Section 3 and Table 1).

Once $P(k)$ is known, we use the Press–Schechter (PS) formalism (Press & Schechter 1974; Mo et al. 2010) with a Gaussian window function to calculate the halo mass function (HMF), $dn(M,z)/dM$, including corrections for ellipsoidal dynamics (Sheth & Tormen 1999). Following Boylan-Kolchin (2022), given the star formation efficiency (SFE), $\epsilon\equiv M_\star/(f_{\rm b}M_{\rm halo})$, we then derive the (comoving) cumulative stellar mass density contained within galaxies above a certain stellar mass $M_\star$ as

$$\rho_\star(>M_\star, z) = \epsilon f_{\rm b}\,\rho(>M_{\rm halo}, z)$$
$$= \epsilon f_{\rm b}\int_{M_{\rm halo}}^{\infty} M\frac{dn(M,z)}{dM}dM, \quad (4)$$

where $f_{\rm b}=\Omega_{\rm b}/\Omega_{\rm m}$ is the cosmic average baryon fraction. Exploring whether PBH scenarios can explain the massive galaxy candidates reported by Labbé et al. (2022), in the following sections we compare the $\rho_\star(>M_\star, z)$ and number density of massive galaxies predicted by our PBH models with observations and discuss the general signatures of PBHs observable by JWST.

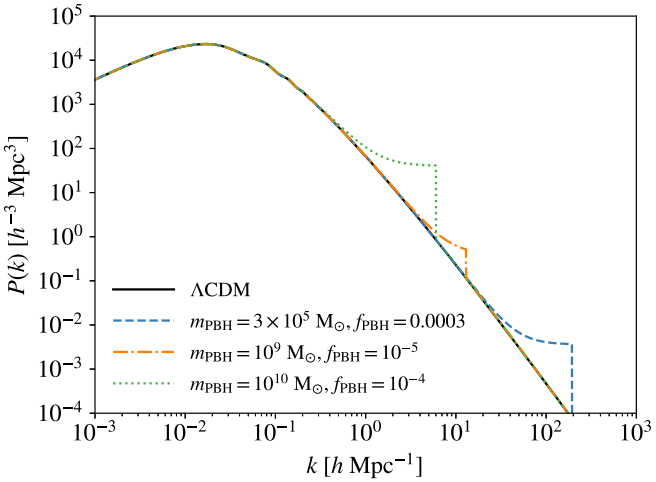

Figure 1. The power spectra of the dark matter density field at $z=0$ in linear perturbation theory for three PBH models with $(m_{\rm PBH}/M_\odot, f_{\rm PBH}) = (3\times10^{-5}, 0.0003)$; (dashed), $(10^9, 10^{-5})$; (dashed–dotted), and $(10^{10}, 10^{-4})$; (dotted), compared with the standard ΛCDM power spectrum (solid) as measured by the Planck Collaboration et al. (2020) from the PYTHON package COLOSSUS (Diemer 2018).

Table 1
Representative PBH Models

Model	$m_{\rm PBH}$ ($M_\odot$)	$f_{\rm PBH}$	$m_{\rm PBH}f_{\rm PBH}$ ($M_\odot$)
M1	3×10^5	0.0003	90
M2	10^9	10^{-5}	10,000
M3	10^{10}	10^{-4}	10^6

[3] The mass spectrum of PBHs can take a variety of forms from different formation mechanisms, as discussed in, e.g., Carr & Silk (2018), Tada & Yokoyama (2019), Carr & Kühnel (2019, 2020), and Carr et al. (2021a). For observational constraints on PBHs, considering an extended mass spectrum of PBHs is a two-edged sword (Carr 2019): on one hand, this tends to make the constraints more stringent in terms of the maximum fraction of dark matter in PBHs from a given mass band (Carr et al. 2017, 2021b). On the other hand, the total PBH density may suffice to explain all dark matter, even if the density in any particular mass band is small and within the observational bounds, as shown in García-Bellido (2019).

[4] We use the ΛCDM power spectrum (for the adiabatic mode) measured by the Planck Collaboration et al. (2020) with $\Omega_{\rm m}=0.3153$, $\Omega_{\rm b}=0.0493$, $h=0.6736$, $\sigma_8=0.8111$, and $n_s=0.9649$ from the PYTHON package COLOSSUS (Diemer 2018).

[5] At early stages when overdensities are very small, the isocurvature mode and adiabatic mode are uncorrelated. However, at later stages (e.g., $z\sim$ 10–20, when the first galaxies form), the two modes can be mixed as PBHs follow the large-scale adiabatic mode to fall into larger structures and meanwhile induce/disrupt dark matter structures around themselves on small scales (Liu et al. 2022).

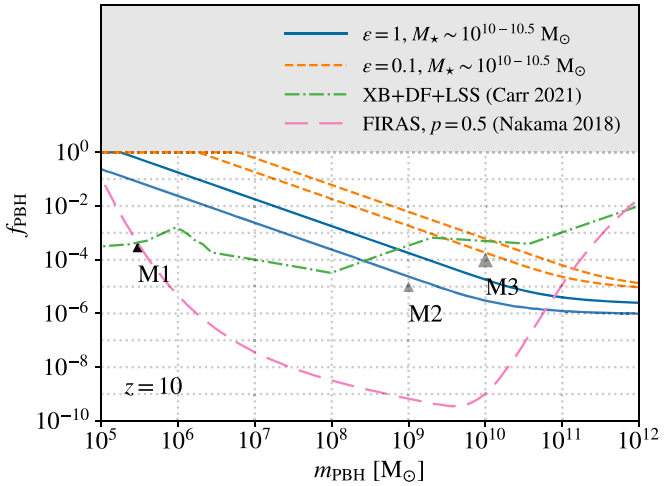

Figure 2. The PBH parameters required to explain the cumulative stellar mass density at $z \sim 10$ measured by JWST (Labbé et al. 2022) with the "Poisson" effect. The PBH models consistent with JWST observations are shown with the solid and dashed curves for $\epsilon = 1$ and 0.1, respectively. In each case, the upper (lower) line corresponds to the data point at the limiting mass $M_\star \sim 10^{10.5\,(10)}$. We also show the constraint from the FIRAS cosmic microwave background μ-distortion limit with a non-Gaussianity parameter $p = 0.5$ (Nakama et al. 2018; long-dashed), and the combined constraint from X-ray binaries (XB, Inoue & Kusenko 2017), dynamical friction (DF, Carr & Sakellariadou 1999), and large-scale structures (LSS, Carr & Silk 2018), compiled by Carr et al. (2021b; dashed–dotted). Three sample models are labeled with triangles (see Table 1), among which the big (small) triangle(s) can(not) explain the JWST results. The darker triangle (M1) satisfies both observational constraints, while the fainter triangles (M2 and M3) only satisfy the XB+DF+LSS constraint.

3. PBH Signatures in the JWST Era

3.1. PBH Models Required to Explain Current JWST Results

Based on 14 galaxy candidates with masses of $\sim 10^9$–$10^{11}\,M_\odot$ at $7 < z < 11$ identified in the JWST CEERS program, Labbé et al. (2022, see their Figure 4) derive the cumulative stellar mass density at $z = 8$ and 10 for $M_\star \gtrsim 10^{10}\,M_\odot$. In particular, they find $\rho_\star(\gtrsim 10^{10}\,M_\odot) \simeq 1.3^{+1.1}_{-0.6} \times 10^6\,M_\odot\ {\rm Mpc}^{-3}$ and $\rho_\star(\gtrsim 10^{10.5}\,M_\odot) \simeq 9^{+11}_{-6} \times 10^5\,M_\odot\ {\rm Mpc}^{-3}$ at $z \sim 10$, higher than the maximum achievable in ΛCDM (with $\epsilon = 1$) by up to a factor of ∼50. Using the formalism described in the previous section (Equations (1)–(4)), we find the PBH parameters that can reproduce these results for SFE values $\epsilon = 1$ and 0.1, comparing with existing observational constraints in the $f_{\rm PBH}$–$m_{\rm PBH}$ space, as shown in Figure 2.

It turns out that, to explain the observational data at $M_\star \sim 10^{10.5\,(10)}\,M_\odot$, we must have $m_{\rm PBH} f_{\rm PBH} \gtrsim 1.8 \times 10^5\,(2.4 \times 10^4)\,M_\odot$ for $\epsilon < 1$ and $m_{\rm PBH} f_{\rm PBH} \gtrsim 6.1 \times 10^6\,(1.8 \times 10^6)\,M_\odot$ for $\epsilon < 0.1$, indicating that we need relatively massive PBHs with $m_{\rm PBH} \gtrsim 10^5\,M_\odot$ since $f_{\rm PBH} \leqslant 1$. To form such massive PBHs in the standard spherical collapse scenario (Escrivà 2022), very large perturbations are required out of inflation, e.g., from non-Gaussian tails produced by interacting quantum fields (e.g., Frampton 2016; Atal et al. 2019; Panagopoulos & Silverstein 2019), or oscillatory features in the inflationary power spectrum (Carr & Kühnel 2019). Such PBH models are strongly constrained by observations of μ-distortion in the cosmic microwave background (CMB), if primordial density fluctuations are Gaussian (Carr et al. 2021b, see their Figures 10 and 16).

Nevertheless, the constraints can be weaker when the Gaussian assumption is relaxed (e.g., Nakama et al. 2018). For instance, with the long-dashed curve in Figure 2 we show a particular case of the phenomenological non-Gaussian model in Nakama et al. (2016) with $p = 0.5$, where p is the non-Gaussianity parameter ($p = 2$ means Gaussian). In this case, PBHs with $m_{\rm PBH} \gtrsim 10^{11}\,M_\odot$ can still have large enough $f_{\rm PBH}$ ($\gtrsim 10^{-5}$) to explain both the JWST observations and the CMB μ-distortion limit (Nakama et al. 2018), as measured by the COBE Far Infrared Absolute Spectrophotometer (FIRAS). However, such models are disfavored by the nondetection of black holes above $10^{11}\,M_\odot$ (except for Phoenix A; Brockamp et al. 2016). Therefore, an even higher degree of non-Gaussianity is required to explain the JWST results with PBH models of $m_{\rm PBH} \lesssim 10^{11}\,M_\odot$ and high enough $f_{\rm PBH}$. Alternatively, the CMB μ-distortion constraint can be evaded if PBHs grow significantly between the μ-distortion epoch ($7 \times 10^6\,{\rm s} < t < 3 \times 10^9\,{\rm s}$) and matter–radiation equality (Carr et al. 2021b), or if PBHs form in nonstandard scenarios such as inhomogeneous baryogenesis with the modified Affleck–Dine mechanism (Kawasaki & Murai 2019; Kasai et al. 2022).

Beyond the μ-distortion constraint, PBHs with $m_{\rm PBH} \gtrsim 10^5\,M_\odot$ are also constrained by X-ray binaries (XB, Inoue & Kusenko 2017), infall of PBHs into the Galactic center by dynamical friction (DF, Carr & Sakellariadou 1999), and large-scale structure statistics (LSS, Carr & Silk 2018), which together require $f_{\rm PBH} \lesssim 10^{-4}$–$10^{-3}$ for $m_{\rm PBH} \sim 10^5$–$10^{11}\,M_\odot$ (see the dashed–dotted curve in Figure 2). Such constraints are generally weaker, allowing a PBH abundance for $m_{\rm PBH} \gtrsim 10^9\,M_\odot$ sufficient to produce the high stellar mass density in massive galaxies at $z \sim 10$ inferred by JWST (Labbé et al. 2022). However, in this regime ($f_{\rm PBH} \lesssim 10^{-3}$), the "seed" effect likely dominates at $z \gtrsim 10$ according to the criterion that the fraction of mass bound to PBHs in the universe is $\ll 1$, i.e., $f_{\rm PBH} \ll (1+z) a_{\rm eq}$ (Carr & Silk 2018). Besides, isocurvature perturbations purely from the "Poisson" effect (without the cutoff in Equation (3)) are strongly constrained by high-z observations (e.g., Sekiguchi et al. 2014; Murgia et al. 2019; Tashiro & Kadota 2021), such that PBH models with $m_{\rm PBH} f_{\rm PBH} \gtrsim 170\,M_\odot$ (and $f_{\rm PBH} > 0.05$) are ruled out by high-z Lyα forest data (Murgia et al. 2019). This motivates us to further explore the "seed" effect.

We perform an idealized calculation to explore what PBH models are needed to form the most massive galaxies observed by JWST purely with the "seed" effect. Assuming that the observed massive galaxies form in halos seeded by PBHs that grow in isolation as $M_{\rm halo} \sim M_{\rm B}(m_{\rm PBH}, z) \sim [(z+1) a_{\rm eq}]^{-1} m_{\rm PBH}$ (Carr & Silk 2018), we require that (i) the average (comoving) number density $\bar{n}_{\rm PBH}$ of PBHs is larger than that of the observed massive galaxies $n_{\rm g} \sim 2 \times 10^{-5}\,{\rm Mpc}^{-3}$ (Boylan-Kolchin 2022; Labbé et al. 2022), and (ii) the PBH-seeded halos have enough gas to form $M_\star \sim 10^{11}\,M_\odot$ of stars, i.e., $\epsilon f_{\rm b} M_{\rm B} = M_\star$ can be satisfied given the limit of ϵ. As shown in Figure 3, we find that the "seed" effect can explain the JWST results with generally less extreme PBH models of $m_{\rm PBH} f_{\rm PBH} \gtrsim 3 \times 10^{5\,(3)}\,M_\odot$ and $m_{\rm PBH} \gtrsim 2 \times 10^{10\,(9)}\,M_\odot$ for $\epsilon \lesssim 0.1\,(1)$. Moreover, considering the nonlinear dynamics around PBH-seeded halos, it is found in cosmological simulations that structures smaller than $\sim M_{\rm B}$ ($\gtrsim 10^{12}\,M_\odot$ at $z \lesssim 10$ for $m_{\rm PBH} \gtrsim 10^9\,M_\odot$) are significantly less abundant than predicted by the "Poisson" effect (Liu et al. 2022, see their Figure 14). This can weaken/lift the Lyα forest constraint that is sensitive for $k \sim 0.7$–$10\,h{\rm Mpc}^{-1}$ (Murgia et al. 2019), corresponding to $M_{\rm halo} \sim 10^9$–$10^{12}\,M_\odot$.

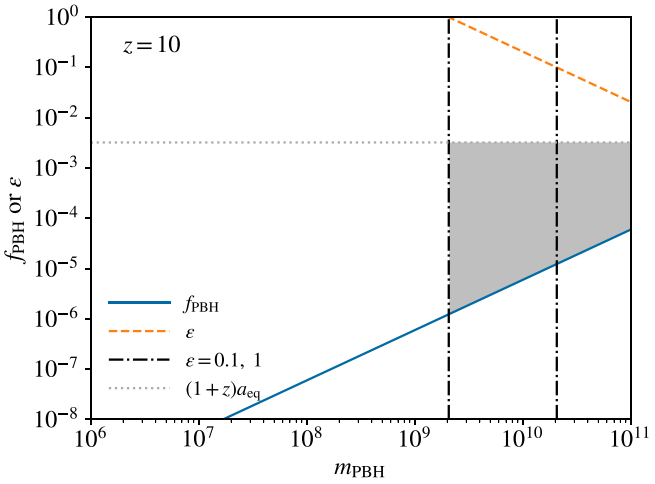

Figure 3. The PBH parameters (shaded region) required to explain the (comoving) number density $n_{\rm g} \sim 2 \times 10^{-5}\,{\rm Mpc}^{-3}$ of observed massive ($M_\star \sim 10^{11}\,M_\odot$) galaxies at $z \sim 10$ (Boylan-Kolchin 2022; Labbé et al. 2022) with the "seed" effect. The shaded region is defined by simple arguments of number counts, baryon mass budget, and the dominance of the "seed" effect: $\bar{n}_{\rm PBH} > n_{\rm g}$ (solid), $\epsilon \equiv M_\star/[f_{\rm b} M_{\rm B}(m_{\rm PBH}, z)] < 1$ (and 0.1, see the dashed and dashed–dotted lines), and $f_{\rm PBH} < (1+z)a_{\rm eq}$ (dotted, which is the general criterion for the assumption that PBHs evolve in isolation to hold; Carr & Silk 2018).

3.2. Signatures of Representative PBH Models

To further demonstrate the effects of PBHs in high-z galaxy/structure formation potentially observable by JWST, we focus on three models representative of typical regions in the PBH parameter space (Figure 2), as listed in Table 1. Here, M1 satisfies all observational constraints considered above, while M2 and M3 only satisfy the XB+DF+LSS combined constraint. For the "Poisson" effect, M3 is consistent with the recent JWST results in Labbé et al. (2022) with $\epsilon \sim 0.1$–1, while M1 and M2 cannot reproduce the observations even with $\epsilon = 1$. For the "seed" effect, M2 can also marginally explain the JWST observations.

In Figure 4, we present the results for $\rho_\star(>M_\star)$ in standard ΛCDM (solid), M1 (dashed), M2 (dashed–dotted), and M3 (dotted) for $\epsilon = 1$ (thin) and 0.1 (thick) at $z = 10$, 15, and 20. We also plot the lower mass limits of galaxies detectable by JWST CEERS NIRCam LW imaging (for an exposure time of ∼2000 s) in Figure 4, considering a magnitude limit of $m_{\rm F444W} \sim 28$ for the filter F444W with a signal-to-noise ratio (SNR) $\gtrsim 5$, derived from the JWST Exposure Time Calculator.[6] We calculate the stellar mass limit as the total mass of stars formed in a star formation event whose peak luminosity matches the magnitude limit according to the stellar population synthesis code YGGDRASIL (Zackrisson et al. 2011). For Population III (Pop III) stars we adopt their (instantaneous-burst) Pop III.1 model with an extremely top-heavy Salpeter initial mass function (IMF) in the range of 50–500 $M_\odot$, based on Schaerer (2002), while for Population II (Pop II) stars we use their $Z = 0.0004$ model from Starburst99 (Leitherer et al. 1999; Vázquez & Leitherer 2005) with a universal Kroupa (2001) IMF in the interval 0.1–100 $M_\odot$. For both Pop III and II, we consider a nebula covering fraction of $f_{\rm cov} = 0.5$ and no Lyα transmission. Note that these limits will be reduced by about one order of magnitude for future deeper surveys with longer (∼100 h) exposures (Zackrisson et al. 2012).

[6] https://jwst.etc.stsci.edu/

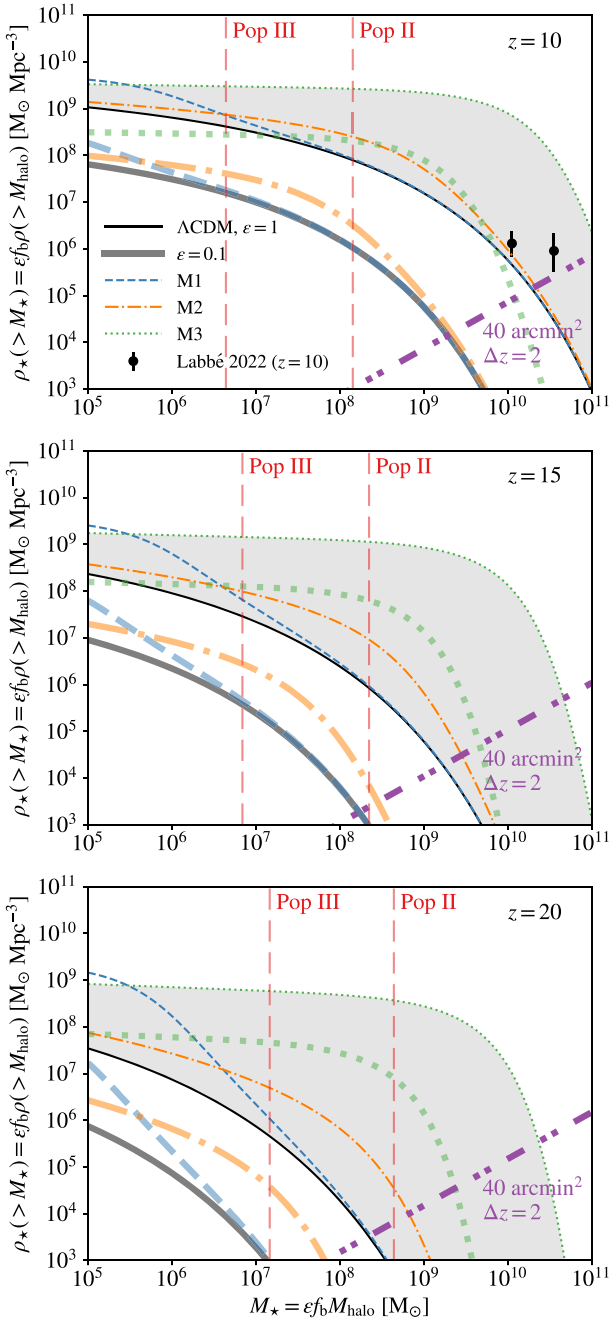

Figure 4. The cumulative (comoving) stellar mass density in galaxies more massive than $M_\star$ at $z = 10$ (top), 15 (middle), and 20 (bottom). The results for standard ΛCDM and PBH models M1, M2, and M3 (see Table 1 and Figure 2) are shown with the solid, dashed, dashed–dotted, and dotted curves for $\epsilon = 1$ (thin) and 0.1 (thick). The shaded region can only be populated by galaxies in PBH cosmologies. The results inferred from the recent JWST observations at $z \sim 10$ (Labbé et al. 2022) are denoted by the data points with error bars. The long-dashed vertical lines mark the lower mass limits of Pop III and II galaxies to be detected by JWST CEERS NIRCam LW imaging (see the main text). We also plot the number count limit $M_\star/V_{\rm com}$ with the dashed–dotted–dotted line, given the comoving volume $V_{\rm com}$ for a survey like CEERS of 40 arcmin^2 and $\Delta z = 2$.

As shown in Figure 4, $\rho_\star(>M_\star)$ can be significantly increased by PBHs, and the effects are the strongest for halos of $M_{\rm halo} \sim m_{\rm PBH}$–$10 m_{\rm PBH}$, and stronger at higher z. In the extreme model M3, the stellar mass budget at $z \lesssim 20$ will be dominated by galaxies more massive than $10^8\,M_\odot$ given $\epsilon \gtrsim 0.1$. Fully taking into account the "seed" effect may further increase

the mass budget of massive halos ($M_{\rm halo} \sim m_{\rm PBH}$–$M_{\rm B}$) with respect to that of the smaller ones (Liu et al. 2022). Even in M1, $\rho_\star(>M_\star)$ is higher by a factor of $\gtrsim$10 than in ΛCDM for $M_\star \sim 10^5\,M_\odot$ at $z \gtrsim 15$. Considering the area (∼40 arcmin^2) of CEERS, corresponding to the number count limit in Figure 4 (i.e., the dashed–dotted–dotted line), we conclude that the fact that JWST has detected galaxies above $10^8\,M_\odot$ at $z \gtrsim 15$ (e.g., Atek et al. 2022; Donnan et al. 2022; Harikane et al. 2022; Naidu et al. 2022; Yan et al. 2022) already requires a very high SFE, $\epsilon \gtrsim 0.1$, for Pop II star formation in ΛCDM, consistent with the UV luminosity function analysis by Inayoshi et al. (2022). That said, for structure formation accelerated by PBHs, such galaxies can also form in more massive halos with a lower SFE (down to 0.01 for M3). Finally, our calculation indicates that at $z \gtrsim 20$ detection of any Pop II galaxy by a survey like CEERS is impossible in ΛCDM, and even Pop III galaxies require $\epsilon \gtrsim 0.1$ to be detected with stellar masses above $10^7\,M_\odot$, which is inconsistent with the theoretical and observational upper limits, $M_{\rm Pop\ III} \lesssim 10^6\,M_\odot$, on the total mass of (active) Pop III stars a halo can host (Yajima & Khochfar 2017; Bhatawdekar & Conselice 2021). However, with massive PBHs like those in M3, it is possible to detect Pop II galaxies as massive as $\gtrsim 4 \times 10^8\,M_\odot$ with $\epsilon \gtrsim 0.01$.

4. Summary and Discussion

The recent detection of surprisingly massive (∼10^{10}–$10^{11}\,M_\odot$) galaxy candidates at $z \sim 10$ by JWST (Labbé et al. 2022), if confirmed, brings new challenges to ΛCDM (and a broad range of dynamical dark energy models) that cannot provide enough baryonic matter in collapsed structures for such early massive galaxy formation (Boylan-Kolchin 2022; Lovell et al. 2022; Menci et al. 2022). Note that the source properties derived from photometry are sensitive to the underlying SED fitting templates, such that the stellar masses can be lower by up to 1.6 dex than reported in Labbé et al. (2022), if other templates with improved physical justifications are adopted, removing the tension with ΛCDM (Steinhardt et al. 2022; see their Figure 3). Currently no template can well match the observed photometry self-consistently, and follow-up spectroscopic observations are needed to robustly pin down the nature and properties of these galaxy candidates (Furlanetto & Mirocha 2022).

Assuming that the results in Labbé et al. (2022) are true and considering only the "Poisson" effect of PBHs, we use a simple analytical model based on linear perturbation theory and the PS formalism to show that such early formation of massive galaxies is possible if PBHs make up part of dark matter with $m_{\rm PBH} f_{\rm PBH} \gtrsim 6 \times 10^6\,(2 \times 10^5)\,M_\odot$ for SFE $\epsilon < 0.1\,(1)$. The "seed" effect, however, requires $m_{\rm PBH} f_{\rm PBH} \gtrsim 3 \times 10^{5\,(3)}\,M_\odot$ and $m_{\rm PBH} \gtrsim 2 \times 10^{10\,(9)}\,M_\odot$ for $\epsilon \lesssim 0.1\,(1)$. Such massive PBHs are mostly ruled out by observations of the CMB μ-distortion, although this strong constraint relies on the assumptions that primordial density fluctuations are Gaussian and that PBHs (formed in the standard scenario of primordial density fluctuations) hardly grow during the radiation-dominated era. Besides, strong isocurvature perturbations purely from the "Poisson" effect of PBHs with $m_{\rm PBH} f_{\rm PBH} \gtrsim 170\,M_\odot$ at scales of $k \sim 0.7$–$10\,h{\rm Mpc}^{-1}$ are ruled out by high-z Lyα forest data (Murgia et al. 2019). Nevertheless, considering the nonlinear dynamics around massive ($m_{\rm PBH} \gtrsim 10^9\,M_\odot$) PBHs, the abundance of halos at such scales can be much lower than predicted by the "Poisson" effect (Liu et al. 2022), lifting the Lyα forest constraint. The μ-distortion constraint can also be evaded by relaxing the underlying assumptions or considering nonstandard PBH formation mechanisms (e.g., Kawasaki & Murai 2019; Kasai et al. 2022). In this way, the other constraints from X-ray binaries (Inayoshi et al. 2022), dynamical friction (Carr & Sakellariadou 1999), and large-scale structures (Carr & Silk 2018) allow for a substantial region in the PBH parameter space with $m_{\rm PBH} \sim 10^9$–$10^{11}\,M_\odot$ and $f_{\rm PBH} \sim 10^{-6}$–10^{-3} that is consistent with the recent JWST observations (and no detection of black holes above $10^{11}\,M_\odot$).

However, considering that PBHs can grow by up to 2 orders of magnitude through the acquisition of dark matter halos by $z \sim 10$ with optimistic spherical[7] accretion (e.g., Mack et al. 2007; De Luca et al. 2020), and the nondetection of black holes above $\sim 10^{11}\,M_\odot$, the allowed region will further shrink. That said, if the stellar masses measured by Labbé et al. (2022) are overestimated (or some of the galaxy candidates are actually at lower z) such that the stellar mass density at $z \sim 10$ is lower in reality, less extreme PBH models would be able to explain them for the same value of ϵ, and the same PBH model could allow lower values of ϵ. For instance, if the inferred stellar masses were indeed reduced by 1.6 dex (Steinhardt et al. 2022) in follow-up observations, we would only need $m_{\rm PBH} f_{\rm PBH} \gtrsim 2 \times 10^5\,M_\odot$ to form the observed galaxies with $\epsilon < 0.025$ from the "Poisson" effect, while the "seed" effect requires $m_{\rm PBH} f_{\rm PBH} \gtrsim 200\,(2)\,M_\odot$ and $m_{\rm PBH} \gtrsim 5 \times 10^{8\,(7)}\,M_\odot$ for $\epsilon \lesssim 0.1\,(1)$.

We also find that the effects of PBHs are stronger at higher z, implying that stronger signatures of PBHs may be found in future wider and deeper surveys by JWST. Actually, if the object CEERS-1749 reported in Naidu et al. (2022) is a galaxy at $z \sim 17$, its large mass ($\sim 5 \times 10^9\,M_\odot$) is also in $>3\sigma$ tension with ΛCDM (Lovell et al. 2022; see their Figure 6). Even if follow-up studies do not find such an excess of very massive galaxies at higher z, this may not necessarily rule out our PBH models, since the SFE can evolve rapidly with redshift at Cosmic Dawn ($z \sim 6$–30) due to metal enrichment, the build-up of radiation backgrounds, and the transition in dominant stellar population (see, e.g., Fialkov & Barkana 2019; Mirocha & Furlanetto 2019; Schauer et al. 2019; Liu et al. 2020). Besides, if the average SFE is not significantly lower with PBHs, the accelerated structure formation leads to accelerated star formation that can also facilitate cosmic reionization. Interestingly, this may explain the recent observations of Lyα emitting galaxies that support a double-reionization scenario with the first full ionization event happening at $z \sim 10$ (Salvador-Solé et al. 2017, 2022). Very massive (∼100–$10^3\,M_\odot$) Pop III stars are required to produce this double-reionization feature in ΛCDM (Salvador-Solé et al. 2017), while less extreme stellar populations may be sufficient with accelerated star formation by PBHs given proper values of SFE.

Note that the PBH masses and the enhancement of density fluctuations by PBHs required to explain the JWST observations in our case ($m_{\rm PBH} \gtrsim 10^9\,M_\odot$ and $m_{\rm PBH} f_{\rm PBH} \gtrsim 3 \times 10^3\,M_\odot$) are significantly higher (and working at larger scales) than those considered by previous studies for stellar-mass PBHs ($m_{\rm PBH} \lesssim 100\,M_\odot$ and $m_{\rm PBH} f_{\rm PBH} \lesssim 30\,M_\odot$; see, e.g., Kashlinsky 2016; Gong & Kitajima 2017; Inman 2019; Cappelluti et al. 2022; Liu et al. 2022). In these studies, the standard picture of first star formation in molecular-cooling minihalos remains

[7] The growth of PBH masses can be much weaker with advection-dominated disk accretion, e.g., up to ∼2% for $m_{\rm PBH} \lesssim 10^7\,M_\odot$ at $z \gtrsim 20$ (Hasinger 2020).

unchanged, but with earlier onset and increased abundances of star-forming halos. However, in our extreme PBH models, star formation may first occur in atomic-cooling halos ($M_{\rm halo} \gtrsim 10^8\,M_\odot$), seeded by PBHs or formed in a top-down fashion by fragmentation of massive ($\gtrsim 10^{11}\,M_\odot$) structures around PBHs. The accretion feedback from black holes can also significantly affect nearby formation of stars and direct collapse black holes (e.g., Pandey & Mangalam 2018; Aykutalp et al. 2020; Liu et al. 2022). Considering the gravitational, hydrodynamic, and radiative effects, early star formation in the presence of massive PBHs can leave strong imprints in the CMB, 21 cm signal, reionization, cosmic infrared, and X-ray backgrounds (see, e.g., Sekiguchi et al. 2014; Kashlinsky 2016; Gong & Kitajima 2017; Murgia et al. 2019; Hasinger 2020; Tashiro & Kadota 2021; Cappelluti et al. 2022; Minoda et al. 2022). These important aspects involving nonlinear dynamics and baryonic physics are beyond the scope of our exploratory work. Follow-up studies with more detailed modeling of the interactions between PBHs, baryons, and (non-PBH) dark matter (in cosmological simulations) are required to fully understand the roles played by massive PBHs in structure/galaxy/star formation and evaluate the viability of such PBH models.

In general, the recent discovery of potentially very early massive galaxy formation by JWST (Labbé et al. 2022) hints at faster structure formation in the high-z universe, above the ΛCDM baseline (Boylan-Kolchin 2022; Lovell et al. 2022), which can be achieved if a small fraction ($\sim 10^{-6}$–10^{-3}) of dark matter is composed of massive ($\gtrsim 10^9\,M_\odot$) PBHs, although more work needs to be done to check whether such fast structure formation is consistent with other observations of the high-z Universe. A similar trend is also seen in observations of (proto-) galaxy clusters that show an excess of strong-lensing sources (Meneghetti et al. 2020, 2022) and of star formation (Remus et al. 2022) that are difficult to explain in ΛCDM. Strikingly, this trend for accelerated structure formation at high z goes in the opposite direction to that of invoking the suppression of fluctuations to account for the well-known small-scale problems of ΛCDM. Together with other hints for PBHs (see, e.g., Clesse & García-Bellido 2018), these findings imply that the nature of dark matter may be more complex than our standard expectation, e.g., involving important subcomponents such as PBHs. This challenge calls for the thorough theoretical exploration of the alternatives to ΛCDM, in conjunction with advanced observational campaigns to probe the high-redshift universe. Here, we are entering an exciting period of discovery with frontier facilities such as JWST, Euclid, and the Square Kilometre Array, as well as the Einstein Telescope and Laser Interferometer Space Antenna gravitational wave observatories.

We would like to thank Antonio Riotto and the anonymous referee for their helpful comments.

ORCID iDs

Boyuan Liu https://orcid.org/0000-0002-4966-7450
Volker Bromm https://orcid.org/0000-0003-0212-2979

References

Afshordi, N., McDonald, P., & Spergel, D. N. 2003, ApJL, 594, L71
Atal, V., Garriga, J., & Marcos-Caballero, A. 2019, JCAP, 2019, 073
Atek, H., Shuntov, M., Furtak, L. J., et al. 2022, arXiv:2207.12338
Aykutalp, A., Barrow, K. S. S., Wise, J. H., & Johnson, J. L. 2020, ApJL, 898, L53
Barkana, R., & Loeb, A. 2001, PhR, 349, 125
Bhatawdekar, R., & Conselice, C. J. 2021, ApJ, 909, 144
Boylan-Kolchin, M. 2022, arXiv:2208.01611
Brockamp, M., Baumgardt, H., Britzen, S., & Zensus, A. 2016, A&A, 585, A153
Bromm, V., & Yoshida, N. 2011, ARA&A, 49, 373
Bullock, J. S., & Boylan-Kolchin, M. 2017, ARA&A, 55, 343
Cappelluti, N., Hasinger, G., & Natarajan, P. 2022, ApJ, 926, 205
Carr, B. 2019, in Illuminating Dark Matter, ed. R. Essig, J. Feng, & K. Zurek (Berlin: Springer), 29
Carr, B., Clesse, S., & García-Bellido, J. 2021a, MNRAS, 501, 1426
Carr, B., Kohri, K., Sendouda, Y., & Yokoyama, J. 2021b, RPPh, 84, 116902
Carr, B., & Kühnel, F. 2019, PhRvD, 99, 103535
Carr, B., & Kühnel, F. 2020, ARNPS, 70, 355
Carr, B., Raidal, M., Tenkanen, T., Vaskonen, V., & Veermäe, H. 2017, PhRvD, 96, 023514
Carr, B., & Silk, J. 2018, MNRAS, 478, 3756
Carr, B. J., & Rees, M. J. 1984, MNRAS, 206, 801
Carr, B. J., & Sakellariadou, M. 1999, ApJ, 516, 195
Clesse, S., & García-Bellido, J. 2018, PDU, 22, 137
Couchman, H. M. P., & Rees, M. J. 1986, MNRAS, 221, 53
De Luca, V., Franciolini, G., Pani, P., & Riotto, A. 2020, JCAP, 2020, 044
Diemer, B. 2018, ApJS, 239, 35
Donnan, C. T., McLeod, D. J., Dunlop, J. S., et al. 2022, arXiv:2207.12356
Escrivà, A. 2022, Univ, 8, 66
Ferrara, A., Pallottini, A., & Dayal, P. 2022, arXiv:2208.00720
Fialkov, A., & Barkana, R. 2019, MNRAS, 486, 1763
Finkelstein, S. L., Bagley, M. B., Arrabal Haro, P., et al. 2022, arXiv:2207.12474
Frampton, P. H. 2016, MPLA, 31, 1650064
Furlanetto, S. R., & Mirocha, J. 2022, arXiv:2208.12828
García-Bellido, J. 2019, RSPTA, 377, 20190091
Gong, J.-O., & Kitajima, N. 2017, JCAP, 2017, 017
Haiman, Z., Thoul, A. A., & Loeb, A. 1996, ApJ, 464, 523
Harikane, Y., Ouchi, M., Oguri, M., et al. 2022, arXiv:2208.01612
Hasinger, G. 2020, JCAP, 2020, 022
Hui, L., Ostriker, J. P., Tremaine, S., & Witten, E. 2017, PhRvD, 95, 043541
Inayoshi, K., Harikane, Y., Inoue, A. K., Li, W., & Ho, L. C. 2022, arXiv:2208.06872
Inman, D., & Ali-Haïmoud, Y. 2019, PhRvD, 100, 083528
Inoue, Y., & Kusenko, A. 2017, JCAP, 2017, 034
Jaacks, J., Finkelstein, S. L., & Bromm, V. 2018, MNRAS, 475, 3883
Kasai, K., Kawasaki, M., & Murai, K. 2022, arXiv:2205.10148
Kashlinsky, A. 2016, ApJL, 823, L25
Kawasaki, M., & Murai, K. 2019, PhRvD, 100, 103521
Klypin, A., Poulin, V., Prada, F., et al. 2021, MNRAS, 504, 769
Kroupa, P. 2001, MNRAS, 322, 231
Labbé, I., van Dokkum, P., Nelson, E., et al. 2022, arXiv:2207.12446
Leitherer, C., Schaerer, D., Goldader, J. D., et al. 1999, ApJS, 123, 3
Liu, B., Schauer, A. T. P., & Bromm, V. 2020, MNRAS, 495, 1700
Liu, B., Zhang, S., & Bromm, V. 2022, MNRAS, 514, 2376
Lovell, C. C., Harrison, I., Harikane, Y., Tacchella, S., & Wilkins, S. M. 2022, arXiv:2208.10479
Mack, K. J., Ostriker, J. P., & Ricotti, M. 2007, ApJ, 665, 1277
Menci, N., Castellano, M., Santini, P., et al. 2022, arXiv:2208.11471
Meneghetti, M., Davoli, G., Bergamini, P., et al. 2020, Sci, 369, 1347
Meneghetti, M., Ragagnin, A., Borgani, S., et al. 2022, arXiv:2204.09065
Minoda, T., Yoshiura, S., & Takahashi, T. 2022, PhRvD, 105, 083523
Mirocha, J., & Furlanetto, S. R. 2019, MNRAS, 483, 1980
Mo, H., Van den Bosch, F., & White, S. 2010, Galaxy Formation and Evolution (Cambridge: Cambridge Univ. Press)
Murgia, R., Scelfo, G., Viel, M., & Raccanelli, A. 2019, PhRvL, 123, 071102
Naidu, R. P., Oesch, P. A., Setton, D. J., et al. 2022, arXiv:2208.02794
Nakama, T., Carr, B., & Silk, J. 2018, PhRvD, 97, 043525
Nakama, T., Suyama, T., & Yokoyama, J. 2016, PhRvD, 94, 103522
Panagopoulos, G., & Silverstein, E. 2019, arXiv:1906.02827
Pandey, K. L., & Mangalam, A. 2018, JApA, 39, 9
Peebles, P. J. E., & Dicke, R. H. 1968, ApJ, 154, 891
Planck Collaboration, Aghanim, N., Akrami, Y., et al. 2020, A&A, 641, A6
Press, W. H., & Schechter, P. 1974, ApJ, 187, 425
Remus, R.-S., Dolag, K., & Dannerbauer, H. 2022, arXiv:2208.01053
Salvador-Solé, E., Manrique, A., Guzman, R., et al. 2017, ApJ, 834, 49
Salvador-Solé, E., Manrique, A., Mas-Hesse, J. M., et al. 2022, arXiv:2208.10426

Schaerer, D. 2002, A&A, 382, 28
Schauer, A. T. P., Liu, B., & Bromm, V. 2019, ApJL, 877, L5
Sekiguchi, T., Tashiro, H., Silk, J., & Sugiyama, N. 2014, JCAP, 2014, 001
Sheth, R. K., & Tormen, G. 1999, MNRAS, 308, 119
Springel, V., Frenk, C. S., & White, S. D. M. 2006, Natur, 440, 1137
Steinhardt, C. L., Kokorev, V., Rusakov, V., Garcia, E., & Sneppen, A. 2022, arXiv:2208.07879
Sullivan, J. M., Hirano, S., & Bromm, V. 2018, MNRAS, 481, L69
Tada, Y., & Yokoyama, S. 2019, PhRvD, 100, 023537
Tashiro, H., & Kadota, K. 2021, PhRvD, 104, 063522
Vázquez, G. A., & Leitherer, C. 2005, ApJ, 621, 695
Yajima, H., & Khochfar, S. 2017, MNRAS, 467, L51
Yan, H., Ma, Z., Ling, C., et al. 2022, arXiv:2207.11558
Zackrisson, E., Rydberg, C.-E., Schaerer, D., Östlin, G., & Tuli, M. 2011, ApJ, 740, 13
Zackrisson, E., Zitrin, A., Trenti, M., et al. 2012, MNRAS, 427, 2212